

Illumination Adaptive Transformer

Ziteng Cui^{1,2}, Kunchang Li², Lin Gu^{1,3}, Shenghan Su⁴, Peng Gao²,
Zhengkai Jiang⁵, Yu Qiao², and Tatsuya Harada^{1,3}

¹ The University of Tokyo

² Shanghai AI laboratory

³ RIKEN AIP

⁴ Shanghai Jiao Tong University

⁵ Tencent YouTu Lab

Abstract. Challenging illumination conditions (low light, underexposure and overexposure) in the real world not only cast an unpleasant visual appearance but also taint the computer vision tasks. Existing light adaptive methods often deal with each condition individually. What is more, most of them often operate on a RAW image or over-simplify the camera image signal processing (ISP) pipeline. By decomposing the light transformation pipeline into local and global ISP components, we propose a lightweight fast Illumination Adaptive Transformer (IAT) which comprises two transformer-style branches: local estimation branch and global ISP branch. While the local branch estimates the pixel-wise local components relevant to illumination, the global branch defines learnable queries that attend the whole image to decode the parameters. Our IAT could also conduct both object detection and semantic segmentation under various light conditions. We have extensively evaluated IAT on multiple real-world datasets on 2 low-level tasks and 3 high-level tasks. With only 90k parameters and 0.004s processing speed (excluding high-level module), our IAT has consistently achieved superior performance over SOTA. Code is available at <https://github.com/cuiziteng/Illumination-Adaptive-Transformer>.

Keywords: Lightness Adaptation · Transformer · Low Light Vision

1 Introduction

Computer vision has witnessed great success on well-taken images and videos. However, the varying light condition in the real world poses challenges on both visual appearance and downstream computer vision tasks (*e.g.*, semantic segmentation and object detection). Images under inadequate illumination (Fig.1) suffer from limited photon counts and undesirable in-camera noise. On the other hand, outdoor scenes are often exposed to strong light such as direct sunlight, making image saturated due to the limited range of sensors and non-linearity in the camera image pipeline. To make it worse, both the under and over exposure may exist together, *i.e.* spatial-variant illumination cast by shadow could make the contrast ratio to be 1000:1 or higher.

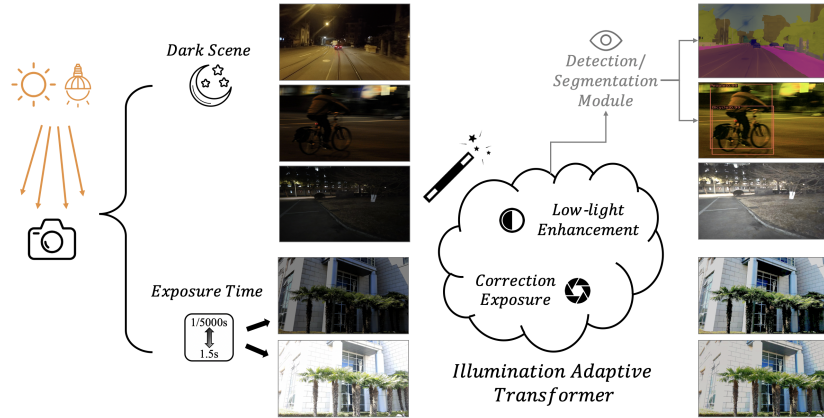


Fig. 1. *Nature lay hid in Night, apply our IAT, and all was light.*

Multiple techniques such as low-light enhancement [37,59,25,47,52,48,24,73,35,62], exposure correction [69,1] have been proposed to adapt to the difficult light condition. Low-light enhancement methods restore the details while suppressing the accompanying noises. Exposure correction focus on adjusting the under and over exposure condition to reconstruct a clear image against strong illumination changes. While the fore-mentioned algorithms focus on improving human oriented visual perceptual, there are also several methods that integrate the enhancement into the high-level tasks such as object detection to boost the robustness against low light [46,16,43,52] and over-exposure conditions [49]. In this paper, we aim to propose a unified lightweight framework to solve these low-level and high-level tasks in the real world.

As shown in Fig.1, left hand side RGB images in Fig.1 suffers non-perfect illumination. However, the intensity of these images is not linearly proportion to the actual scene irradiance due to the image signal processor (ISP) pipeline in the camera. Since it is not straightforward to transfer these images to the normal-lit RGB ones, existing methods either directly operate on RAW images [9,3] or over-simplify the ISP pipeline with gamma correction [48] etc.

In this work, we analyze a pipeline that transfers the input RGB image through an inverse ISP to RAW and then converts the adapted normal-lit RAW image into target RGB. It shows that this pipeline could be decomposed into a combination of pixel-wise local components and global ISP components. Based on the analysis, we propose a Illumination Adaptive Transformer (IAT), shown in Fig.1, which also consists of two transformer-style branches. Both branches are designed to be lightweight to estimate the factors for generating the adapted RGB images. The local branch estimates the pixel-wise local components relevant to illumination, wherein the input resolution is maintained to preserve the informative details. The global branch estimates global ISP parameters by designing the learnable queries to attend the whole image. Furthermore, via attaching a high-level task module, we could jointly optimize our IAT for object detection and semantic segmentation under challenging light conditions.

Extensive experiments are conducted on several real-world datasets, *i.e.*, LOL [65] and FiveK [6] for low-level tasks, and EXDark [46], ACDC [56] and TYO-L [29] for high-level tasks. Results show that our IAT can achieve state-of-the-art performance across a range of tasks. More importantly, our IAT only contains **0.09M** model parameters, which is **100 \times** smaller than current SOTA models (*e.g.*, 14.14M for MAXIM[62]). Besides, its average inference time on LOL benchmark [65] only require **0.004s** per image, while the SOTA methods often take 1s per image.

Our contribution could be summarized as follow:

- We have proposed a fast light-weight framework, Illumination Adaptive Transformer (IAT), to handle challenging light conditions in the real world.
- We have proposed a novel transformer-style structure to estimate global ISP parameters to fuse the RGB target image, wherein the learnable quires are utilized to attend the whole image.
- Extensive experiments on several real-world datasets on 2 low-level tasks and 3 high-level tasks show the superior performance of IAT over SOTA methods. IAT is light-weight and mobile-friendly with only **0.09M** model parameters and **0.004s** processing time per image. We will release the source code upon publication.

2 Related Works

2.1 Enhancement against Challenging Light Condition

Low-light Enhancement. Earlier low-light image enhancement solutions use RetiNex theory [37] based methods and histogram equalization [22,59] based methods. Since LLNet [47] first utilize a deep-autoencoder structure, deep-learning based methods [48,73,72,35,24,74,51,64,62,20] have been widely used in this task and gain SOTA results on the benchmark enhancement datasets [6,65].

Image enhancement is also relevant to multi-illuminant estimation that corrects the undesired colour cast by light. Assuming illumination varies smoothly across the image, the spatially varying illuminants could be estimated [19,37]. Making use of the local information, [21,23] cluster the local features to group independent illuminants. Deep learning solutions have also gained attention. For example, Bianco *et al.* [3] directly apply CNN on the RAW data for the estimation of both single and multiple illumination.

Exposure Correction. Similarly to Low-light enhancement, traditional exposure correction algorithms [38,8] also use image histograms to adjust image intensities. Another strategy corrects exposure errors by adjusting the tone curve via a trained deep learning model [68,53]. Very recently, Afifi *et al.* [1] proposed a coarse-to-fine neural network to correct exposure of photo.

High-level Task. Existing high-level vision frameworks [7,54,12,45] are trained on large scale normal-light datasets (*i.e.* MS COCO [42], ImageNet [17]). Facing the challenging lighting conditions, directly taking low-light/strong-light data as

input would suffer lightness inconsistency [66,43], thus deteriorating the performance. Another solution is pre-processing the images with enhancements methods [48,73,51] before conducting the detection [54,7] or segmentation [12]. However, due to the target inconsistency [52,16,44], most of the enhancement methods are designed to improve human visual perception, which may not necessarily benefit the high-level tasks.

To handle this issue, YOLO-in-the-dark [57] built a teacher-student model to offset the gap between low-light RAW and normal-light RGB for low-light RAW object detection. MAET [16] proposes a low-light data synthesis method and uses self-supervised learning strategy [71] to train the object detector for low-light object detection. DB-GAN [49] uses GAN for image normalization, then jointly trains the GAN model and object detector to handle object detection under strong light environments.

2.2 Vision Transformers

Since ViT [18], Transformer based model has gained superior performances in many computer vision tasks, including image classification [45], object detection [7] and so on. For low-level vision tasks, transformer-based models have made much progress on several tasks, such as image super-resolution [41], image restoration [70], image colorization [36], image enhancement [74] and bad weather restoration [10,63]. Besides, the MLP-Mixer [58,60] based method [62] also shows MLP model's potential on low-level vision tasks. However, directly using a transformer as an image-to-image structure would bring too much computation cost, making it hard to build a transformer model on mobile and edge devices.

3 Illumination Adaptive Transformer

3.1 Light Adaption Model

For an RGB image I_i under spatial variable light L_i , the light adaption model maps it to target RGB image I_t (under light L_t) that matches the real photo. Existing methods tend to follow an over-simplified model, either linear or only considering the gamma correction [48]. However, the actual processing in camera involves more elaborated non-linear operations such as demosaicing, white balance, colour space transform, gamma correction, etc. This is called image signal processor (ISP) pipeline, which transforms original RAW images, which is linearly proportional to scene irradiance, to RGB images used in computer vision datasets and tasks. Existing illumination estimation or enhancement methods [3,9] often chose to directly operate on RAW data rather than RGB images, thus inevitably limiting the application scope.

Brooks *et al.* [5] shows that an invertible and bijective function $f(\cdot)$ could be defined to map data point in RAW data space to RGB space. As shown on the right hand side of Fig.2, the input RGB image $I_i(x)$ of colour channel $c \in \{r, g, b\}$

at pixel x is at first mapped to RAW space $R_i(x)$ with an inverse ISP procedure:

$$R_i(x, c) = f^{-1}(I_i(x), c). \quad (1)$$

On RAW dataspace, $R_i(x)$ of pixel x is then linearly adapted to target $R_t(x)$ under target light L_t following von Kries coefficient law [4]:

$$R_t(x, c) = \frac{L_t(x, c)}{L_i(x, c)} R_i(x, c). \quad (2)$$

Based on [5,13,16], our ISP pipeline follows the following order: demosaicing, white balance, colour space transformation and gamma correction. Therefore, the ISP function f could be further decomposed into

$$f(\cdot, c_i) = \left(\sum_{c_j} k_{c_i, c_j} (D(\cdot)) \right)^\gamma, c_i, c_j \in \{r, g, b\}, \quad (3)$$

where $D(\cdot)$ represents the transformation of demosaicing and some denoising operations. The W represents the colour transfer matrix that combines camera colour space transformation and white balance operation. γ represents gamma value in gamma correction.

The target RGB image $I_t(x, c_i)$ of channel c_i then becomes:

$$I_t(x, c_i) = \left(\sum_{c_j} k_{c_i, c_j} D \left(\frac{L_t(x)}{L_i(x)} f^{-1}(I_i(x, c_i)) \right) \right)^\gamma \quad (4)$$

$$= \left(\sum_{c_j} W_{c_i, c_j} (M_{c_i}(x) I_i(x, c_i) + A_{c_i}(x)) \right)^\gamma \quad (5)$$

We simplify the complex and non-linear transformation of Eq.1 and $D(\cdot)$ into a combination of multiplier factor $M(x)$ and additive $A(x)$. The spatial distribution of light L is widely assumed to be varying smoothly without abrupt changes between adjacent locations [37,19]. Since the pixel-wise factors $M(x)$ and $A(x)$ depend on local information of $L_t(x)$ and $L_i(x)$ and global configuration of ISP procedure, the pixel value $M(x)$ and $A(x)$ should also vary smoothly across the space, leaving a small degree of freedom on spatial distribution.

3.2 Model Structure

Given an input RGB image $I_i \in \mathbb{R}^{H \times W \times 3}$ under light condition L_i , where $H \times W$ denotes the size dimension and 3 deotes the chanel dimension ($\{r, g, b\}$). As shown in Fig.2, we propose our Illumination Adaptive Transformer (IAT) to transfer the input RGB image I_i to a target RGB $I_t \in \mathbb{R}^{H \times W \times 3}$ under the proper uniform light L_t . By incorporating the downstream detection or segmentation module [7,54,12], our IAT could also achieve high-level vision tasks under different illumination environments.

According to the discussion above, the complex pipeline, as shown in Fig.2, that transfers RGB image I_i to RGB image I_t , could be simplified into Eq.5. The

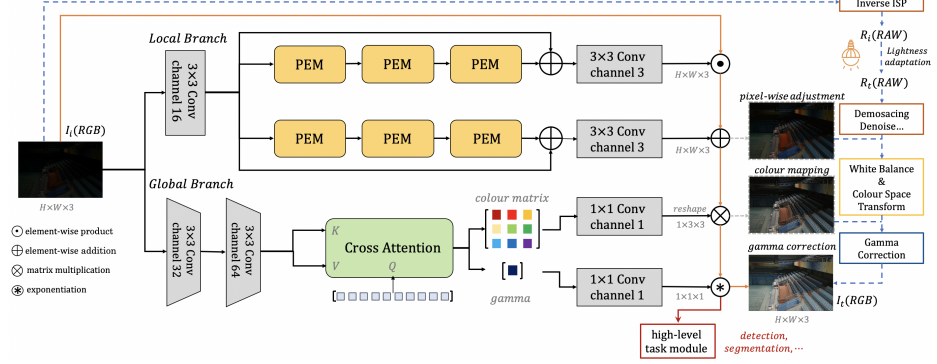


Fig. 2. Structure of our Illumination Adaptive Transformer (IAT), the black line refers to the parameters generation while the yellow line refers to image processing. The light adaption pipeline is shown on the right hand side.

non-linear operations are decomposed into local pixel-wise components $M, A \in \mathbb{R}^{H \times W \times 3}$ and global ISP components $W \in \mathbb{R}^{3 \times 3}, \gamma \in \mathbb{R}^{1 \times 1}$. Thus, we design two transformers style branches: local branch and global ISP branch to estimate the local pixel-wise components and global ISP components respectively.

As shown in Fig. Fig.2, our ISP obtains the target RGB image I_t via

$$I_t = ((concat(I_i \odot M + A))W)^\gamma. \quad (6)$$

concat is an operation concatenates $I_i \odot M + A$ into HW matrix. The exponential operations here is also point wise.

Local Branch. In the local branch, we focus on estimating the local components M, A to correct the effect of illumination following Eq.5. Instead of adopting a U-Net [55] style structure, which downsamples the images first before upsampling them, we aim to maintain the input resolution through the local branch to preserve the informative details. Therefore, we propose a novel transformer-style architecture for the local branch. Compared to the popular U-Net [55] style structure, our structure could also deal with arbitrary resolution images without resizing them.

At first, we expand the channel dimension via a 3×3 convolution and pass them to two independent branches stacked by Pixel-wise Enhancement Module (PEM). Since M and A should vary smoothly on the spatial domain as discussed in Section 3.1, in our Pixel-wise Enhancement Module (PEM), we replace self-attention with depth-wise convolution as suggested in the previous works [26, 40, 39]. As shown in Fig. 3(a), our PEM first encode the position information by 3×3 depth-wise convolution before enhancing local details with PWConv-DWConv-PWConv. Finally, we adopt two 1×1 convolutions to enhance token representation individually. Specially, we design Colour Normalization to replace Layer Normalization [2]. It learns to scale a and bias b via two learnable parameters, and fuses the channels via the learnable matrix, which is initiated as an

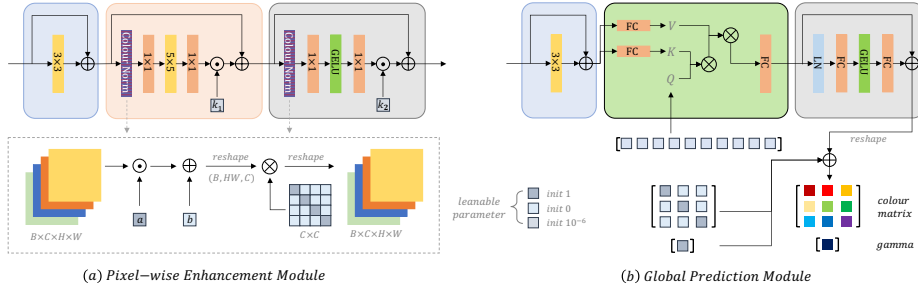


Fig. 3. Detailed structure of Pixel-wise Enhancement Module (PEM) and Global Prediction Module (GPM).

identity matrix. Besides, we adopt Layer Scale [61] for better convergence, which multiplies the features by a small number k_1/k_2 .

We stack 3 PEMs in each branch and then connect the output features with the input features through element-wise addition. This skip connection [27] helps maintain the original image details. Finally, we decrease the channel dimension by a 3×3 convolutions and adopt ReLU/Tanh function to generate the local components M/A in Eq. 5.

Global ISP Branch. Global ISP branch accounts for part of the ISP pipeline [28,32,34,5] (*i.e.* gamma correction, colour matrix transform, white balance) when transferring the target RGB image I_t . Specifically, the value of each pixel in the target image is determined by a global operation defined in Eq. 5.

Inspired by Detection Transformer DETR [7] that uses object queries to decode the position and labels, we also design global component queries to decode and predict the W, γ and then apply it to generate RGB image I_t . This transformer structure allows capturing global interactions between context and individual pixels. As shown in Fig. 2, we first stack two convolutions as a lightweight encoder, which encodes the features in a high dimension with lower resolution. Then the features are passed to the Global Prediction Module (GPM), for effective global modeling. As shown in Fig. 3(b), different from DETR, our global component queries Q are initialized as zeros without extra multi-head self-attention. Q is global component learnable embedding that attends keys K and values V generated from encoded features. The positional encoding for K and V is from a depth-wise convolution, which is friendly with different input resolutions. After FFN with two linear layers [18], we add two extra parameters with special initialization to output colour matrix and gamma. Such initialization makes sure the colour matrix is identity matrix W and the gamma value g is one in the beginning, thus contributing to stable training.

3.3 High-level Vision

As shown in Fig. 4, by passing I_t to the attached downstream task module, our IAT could conduct object detection and semantic segmentation. During train-

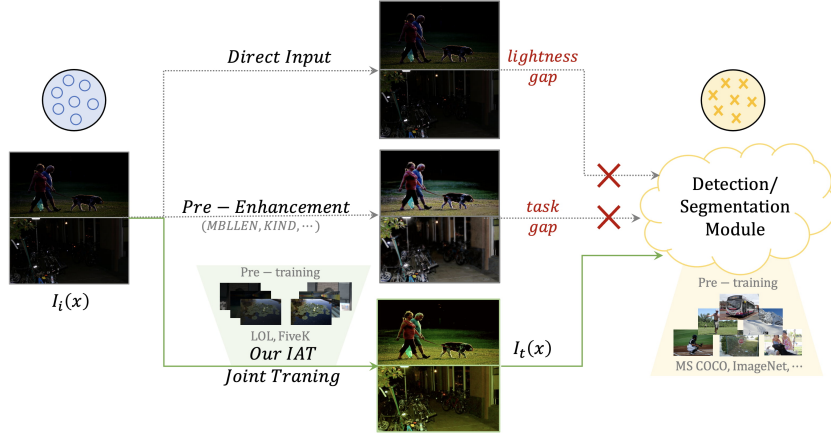


Fig. 4. IAT for high-level vision.

ing, we aim to minimise the downstream framework’s loss function (*i.e.* object detection loss L_{obj} between prediction \hat{t} and ground truth t) by jointly optimising the whole network’s parameters (see Eq. 7). Compared to the subsequent high-level module, the time-complexity and model storage of our IAT main structure could be ignored (*i.e.* IAT main structure *v.s.* YOLO-V3 [54], 417KB *v.s.* 237MB).

$$\min_{i \in \mathbb{I}, d \in \mathbb{D}} L_{obj}(\hat{t}, t) \quad (7)$$

$$I_t(x) = \mathbb{I}(I_1(x)), \quad \hat{t} = \mathbb{D}(I_t(x))$$

4 Experiments

We evaluate our proposed IAT model on benchmark datasets and experimental settings for both low-level and high-level vision tasks under different illumination conditions. Three low-level vision tasks include: (a) image enhancement (LOL [65]), (b) image enhancement (MIT-Adobe FiveK [6]), (c) exposure correction [1]. Three high-level vision tasks include: (d) low-light object detection (e) low-light semantic segmentation (f) various-light object detection. The PEM number in local branch to generate M and A are both set to 3, while the channel number in PEM is set to 16.

For all low-level vision experiments: $\{(a), (b), (c)\}$, the IAT model are trained on a single GeForce RTX 3090 GPU with batch size 8. We use Adam optimizer to train our IAT model while the initial learning rate and weight decay are separately set to $2e^{-4}$ and $1e^{-4}$. A cosine learning schedule has also been adopted to avoid overfitting. For data augmentation, horizontal and vertical flips have been used to acquire better results.

4.1 Image Enhancement Results

For (a) and (b) image enhancement task, we evaluate our IAT framework on two benchmark real-world datasets: LOL [65] and MIT-Adobe FiveK [6].

LOL [65] is a small dataset consisting of 789 paired normal-light images and low-light images. 689 images are used for training and the other 100 images are for testing. The loss function between input image I_i and target image I_t for LOL dataset training is a mixed loss function [63] which consists of smooth L1 loss and VGG loss [33]. As shown in Eq. 8, λ is a weight parameter which set to 0.04 in our experiments. In both training and testing, the image resolution is maintained at 600×400 . We compare our method with SOTA low light enhancement methods [25,65,48,73,24,67,72,62,35]. For image quality analysis, we evaluate three metrics: peak signal-to-noise ratio(PSNR), structural similarity index measure (SSIM) and NIQE [50]. To analyse the computational complexity, we also report three metrics: FLOPs, model parameters and test time shown in the last column of Table.1. We have listed different model's test time on their corresponding code platform (M means Matlab, T means TensorFlow, P means PyTorch). As shown in Table 1, **IAT(local)** means only using the local network to train the model and **IAT** means using the whole framework. We could see that our **IAT** gains SOTA result on both image quality and computational complexity.

$$L_{mix}(I_1, I_2) = L_{smoothL1}(I_1, I_2) + \lambda \cdot L_{vgg}(I_1, I_2)$$

$$L_{smoothL1}(I_1, I_2) = \begin{cases} 0.5 \cdot (I_1 - I_2)^2, & |I_1 - I_2| < 0 \\ |I_1 - I_2| - 0.5, & \text{otherwise} \end{cases} \quad (8)$$

MIT-Adobe FiveK [6] dataset contains 5000 images, each of which was manually enhanced by five different experts (A/B/C/D/E). Following the previous settings [64,74,51], we only use experts C's adjusted images as ground truth images. For MIT-Adobe FiveK [6] dataset training, we use a single L1 loss function to optimize IAT model. We compare our method with SOTA enhancement methods [30,55,14,31,64,64,51,74] on FiveK dataset, then report image quality results (PSNR,SSIM) and model parameters in Table. 2. Our **IAT** also gain satisfactory result in both quality and efficiency. Qualitative results of LOL [65] and FiveK [6] has been shown in Fig.5, more results are in supplementary.

4.2 Exposure Correction Results

For the (c) exposure correction task, we evaluate IAT on the benchmark dataset proposed by [1]. The dataset contains 24,330 8-bit sRGB images, divided into 17,675 training images, 750 validation images, and 5905 test images. Images in [1] are adjusted by MIT-Adobe FiveK [6] dataset with 5 different exposure values (EV), ranging from under-exposure to over-exposure condition. Same as [6], test set has 5 different experts' adjust results (A/B/C/D/E). Following the setting of [1], the training images are cropped to 512×512 patches and the test image is resized to have a maximum dimension of 512 pixels. we compare the test images

Table 1. Experimental results on LOL [65] dataset, best and second best results are marked in red and blue respectively, noted here [25] is non-deep learning method and [24] is self-supervised learning method.

Method	PSNR↑	SSIM↑	NIQE↓	FLOPs(G)↓	#Params.(M)↓	test time(s)↓
LIME* [25]	14.92	0.516	5.77	-	-	3.241 (M)
Zero-DCE* [24]	14.83	0.531	8.22	2.53	0.08	0.002 (P)
RetiNexNet [65]	16.77	0.562	8.89	136.01	0.84	0.841 (T)
MBLLEN [48]	17.90	0.702	7.82	19.95	20.47	2.981 (T)
DRBN [67]	20.13	0.820	5.11	37.79	0.58	1.210 (P)
KIND [73]	20.86	0.810	5.15	29.13	8.16	0.138 (T)
KIND++ [72]	21.30	0.822	3.88	-	8.28	1.013 (T)
RCT [35]	22.67	0.788	-	-	-	-
MAXIM [62]	23.43	0.863	-	216.00	14.14	-
IAT (local)	20.30	0.789	4.03	1.31	0.02	0.002 (P)
IAT	23.50	0.824	3.08	1.44	0.09	0.004 (P)

Table 2. Experimental results on MIT-Adobe FiveK [6] dataset.

Metric	White-Box [30]	U-Net [55]	DPE [14]	DPED [31]	D-UPE [64]	D-LPF [51]	STAR [74]	IAT
PSNR↑	18.57	21.57	23.80	21.76	23.04	23.63	24.50	24.88
SSIM↑	0.701	0.843	0.880	0.871	0.893	0.875	0.893	0.905
#Params.↓	-	1.3M	3.3M	-	1.0M	0.8M	0.02M	0.09M

with all five experts’ results. Here we use the mixed loss function (Eq. 8) for exposure correction training.

The evaluation result have been shown in Table. 3, our comparison methods include both traditional image processing methods (Histogram Equalization [22], LIME [25]) and deep learning methods (DPED [31], DPE [14], RetinexNet [65], Deep-UPE [64], Zero-DCE [24], MSEC [1]). Evaluation metrics are same as [1], including PSNR, SSIM and perceptual index(PI). Table. 3 shows that our **IAT** model has gained best result on all evaluation indexs. Also compared to the second best result MSEC [1], IAT has much fewer parameters (0.09M v.s. 7M) and less evaluation time (0.004s per image v.s. 0.5s per image). Qualitative result has been shown in Fig.5, more results are in supplementary.

4.3 Performance of High-level Vision

For the high-level vision tasks: $\{(d), (e), (f)\}$, we build our code on mmdetection and mmsegmentation frameworks [11,15]. For a fair comparison, we take all the experiments in the same setting: same input size, same data augmentation methods (expand, random crop, multi-size, random flip...). All the models are initialed with COCO [42] pre-trained weight.

Low-Light Object Detection. We first evaluate the (d) low-light object detection task on the benchmark real-world dataset EXDark [46]. EXDark includes 7,363 real-world low-light images, ranging from twilight to extreme dark environment with 12 object categories. Similar to the setting of [16], we take 80% images of each category for training and the other 20% for testing. We choose both CNN-based detector YOLO-V3 [54] and transformer-based detector DETR [7] for evaluation. For YOLO-V3 [54] training, all the input images

Table 3. Experimental results on exposure correction dataset [1], note here HE and LIME [25] are non-deep learning methods. PSNR, SSIM and PI results, reported by competing works, are replicated from [1].

Method	Expert A		Expert B		Expert C		Expert D		Expert E		Avg		PI \downarrow
	PSNR \uparrow	SSIM \uparrow											
HE* [22]	16.14	0.685	16.28	0.671	16.52	0.696	16.63	0.668	17.30	0.688	16.58	0.682	2.405
LIME* [25]	11.15	0.590	11.83	0.610	11.52	0.607	12.64	0.628	13.61	0.653	12.15	0.618	2.432
DPED [31] (iPhone)	15.13	0.609	16.51	0.636	15.91	0.622	16.57	0.627	17.25	0.649	16.27	0.629	2.903
DPED [31] (Sony)	17.42	0.675	18.64	0.701	18.02	0.683	17.55	0.660	17.78	0.663	17.88	0.676	2.806
DPE [14] (U-FiveK)	16.24	0.653	16.81	0.646	16.84	0.671	16.76	0.654	16.71	0.650	16.67	0.655	2.606
DPE [14] (S-FiveK)	16.93	0.678	17.70	0.668	17.74	0.696	17.57	0.674	17.60	0.670	17.51	0.677	2.621
RetinexNet [65]	10.76	0.585	11.61	0.596	11.13	0.605	11.99	0.615	12.67	0.636	11.63	0.607	3.105
Deep-UPE [64]	13.16	0.610	13.90	0.642	13.69	0.632	14.80	0.649	15.68	0.667	14.25	0.640	2.405
Zero-DCE [24]	11.64	0.536	12.56	0.539	12.06	0.544	12.96	0.548	13.77	0.580	12.60	0.549	2.865
MSEC [1]	19.16	0.746	20.10	0.734	20.20	0.769	18.98	0.719	18.98	0.727	19.48	0.739	2.251
IAT (local)	16.61	0.750	17.52	0.822	16.95	0.780	17.02	0.773	16.43	0.789	16.91	0.783	2.401
IAT	19.90	0.817	21.65	0.867	21.23	0.850	19.86	0.844	19.34	0.840	20.34	0.844	2.249

Table 4. Experiment results on EXDark [46] dataset, the best, second best and third best results are marked in red, blue and green respectively.

Detector	Type	Method	Bicycle	Boat	Bottle	Bus	Car	Cat	Chair	Cup	Dog	Motorbike	People	Table	Total
YOLO-V3[54]	Baseline	-	79.8	75.3	78.1	92.3	83.0	68.0	69.0	79.0	78.0	77.3	81.5	55.5	76.4
	Enhancement	MBLLEN [48]	82.0	77.3	76.5	91.3	84.0	67.6	69.1	77.6	80.4	75.6	81.9	58.6	76.8
	KIND [73]	80.1	77.7	77.2	93.8	83.9	66.9	68.7	77.4	79.3	75.3	80.9	53.8	76.3	
	DeepLPF [51]	81.9	76.0	74.1	90.5	83.4	66.3	71.9	77.2	80.3	77.9	81.7	54.6	76.3	
	Pre-train	MAET [16]	83.1	78.5	75.6	92.9	83.1	73.4	71.3	79.8	77.2	81.1	57.0	77.7	
	Zero-DCE [24]	83.6	78.1	78.2	93.1	84.3	70.4	71.3	77.9	77.2	77.8	80.9	54.8	77.3	
	Joint-train	IAT (None)	81.8	78.0	76.6	93.0	83.6	71.9	69.6	77.6	77.1	77.5	81.5	54.9	77.1
		IAT (LOL)	79.8	76.9	78.6	92.5	83.8	73.6	72.4	78.6	79.0	79.0	81.1	57.7	77.8
		IAT (FiveK)	82.2	78.1	76.2	92.2	84.0	69.1	72.3	78.0	81.1	80.1	82.1	55.4	77.6
	Baseline	-	78.7	72.3	74.9	93.8	81.6	71.2	66.5	72.1	78.9	71.2	79.1	62.1	75.2
DETR [7]	Enhancement	MBLLEN [48]	80.4	75.8	75.6	92.2	82.2	71.4	68.7	72.0	77.6	70.4	78.1	63.4	75.7
	KIND [73]	77.1	76.7	78.5	91.1	82.5	70.2	68.1	70.6	74.2	71.0	79.0	59.8	74.9	
	DeepLPF [51]	77.6	74.1	75.7	95.4	83.1	73.8	69.2	72.4	81.1	68.7	77.9	60.5	75.8	
	Zero-DCE [24]	79.9	76.0	76.9	92.4	82.4	75.3	70.5	73.4	76.3	73.7	80.0	61.4	76.5	
	Joint-train	IAT (None)	77.7	74.6	77.2	93.4	83.2	73.3	70.0	73.8	78.8	72.4	78.6	60.9	76.2
		IAT (LOL)	79.8	76.8	77.5	91.0	82.1	77.8	70.6	71.3	79.3	70.0	79.6	65.0	76.7
		IAT (FiveK)	77.8	74.3	76.4	95.9	83.5	77.7	70.0	72.8	80.9	72.7	78.4	62.1	76.9

have been cropped and resized to 608×608 pixel size, we use SGD optimizer to train YOLO-V3 for 25 epochs with batch size 8. The initial learning rate is $1e^{-3}$, momentum and weight decay is separately set to 0.9 and $5e^{-4}$, and the learning rate is decay to one-tenth at 18 and 23 epoch. For DETR [7] training, the input images are resized with a long side of 1333 pixel size. We use Adam optimizer to train DETR for 20 epochs with batch size 2 while the initial learning rate is $1e^{-4}$. Weight decay is $1e^{-4}$ and the learning rate is decay to one-tenth at 14 and 20 epochs.

The comparison methods include several types: (1). baseline: directly train detectors with EXDark [46] original low-light images, (2). Enhancement: train detectors with EXDark [46] images enhancement by different methods [48,73,51], (3). Pre-train: MAET [16] changes the original pre-train COCO [42] model with low-light pre-train model. (4). Joint-train: joint training the enhancement network and detectors (details in Sec. 3.3). Here we initialize IAT model with different weights in Sec. 4.1 (no pretrain, pretrained on LOL dataset [65], pretrained on MIT-Adobe FiveK dataset [6]) ⁶. Experiment results is reported in Table. 4.

⁶ Zero-DCE [24] model is initialed with their own model weight in <https://github.com/Li-Chongyi/Zero-DCE>.

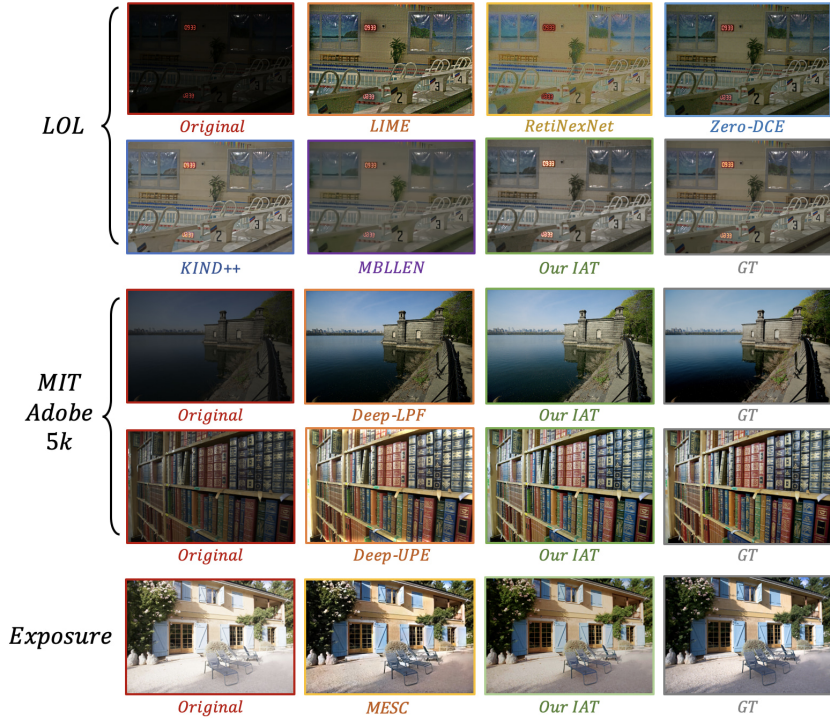


Fig. 5. Results on enhancement dataset [65,6]) and exposure correction dataset [1].

Table 5. Results on ACDC [56] low-light semantic segmentation and TYO-L [29] various-light object detection .

Dataset	Metric	Base	Pre-process			Joint-train			
			HE	MBLLEN	Deep-LPF	IAT (none)	IAT (FiveK)	IAT (LOL)	IAT (exp)
ACDC [56]	mIoU	53.3	50.0	61.8	61.4	61.2	61.9	61.7	-
	time (s)	0.249	0.332	0.807	1.961		0.280		
TYO-L [29]	mAP	88.4	92.4	95.3	94.5	96.7	-	-	96.1
	time (s)	0.023	0.105	0.580	1.023	0.027			0.027

We evaluate each class and total mean average precision (mAP) at IOU 0.5. From Table. 4, we could see that directly using enhancement methods [48,73,51] to pre-process image may be helpful to machine vision. In the joint-train fashion, initialising with pre-train weight on enhancement datasets (LOL [65], MIT-Adobe FiveK [6]) would be helpful to low-light object detection task. Some of the detection results could be seen in Fig.6, we shows the $I_t(x)$ in Eq. 7.

Low-Light Semantic Segmentation. For (e) low-light semantic segmentation task, we use benchmark real-world dataset ACDC’s [56] low-light part for model evaluation. There are total 1006 dark scene images in the ACDC dataset, including 400 for training, 106 for validation and the other 500 for testing. We use DeeplabV3+ [12] segmentation model and the input images are cropped and resized to 512×512 pixel size. The model is trained by SGD optimizer with



Fig. 6. Detection results of DETR [7] on EXDark [46]. (a) is the original images, (b) and (c) are images enhancement by MBLLEN [48] and KinD [73], (d) and (e) are the output of IAT model ($I_t(x)$ in Eq. 7), respectively initialized by LOL[65] and FiveK[6]

batch size 8 for 20000 iters, initial learning rate is set to 0.04, momentum and weight decay are separately 0.9 and $5e^{-4}$.

We compare our method with three enhancement methods: Histogram Equalization [22], MBLLEN [48] and DeepLPF [51], we report mIOU and test time results and total evaluation time in Table. 5. From the results, we could see that our **IAT** framework gains SOTA results on both accuracy and speed. Some qualitative results and the generated images ($I_t(x)$) of IAT have been shown in Fig. 7. In the segmentation task, the **IAT** module is more inclined to learn edge information rather than colour information (see (d) in Fig. 7).

Various Light Object Detection. For (f) various light object detection tasks, we use the real-world dataset Toyota Light (TYO-L) [29]. TYO-L includes 1680 images with 21 classes, each class contains 80 images under five different light conditions. We take 65 images in each class for training and the other 15 images for testing, so the total train set contains 1365 images and the test set contains 315 images. We use YOLO-V3 [54] detector to train the model for 45 epochs, initial learn rate is $1e^{-3}$ and decay to one-tenth at 36 and 42 epoch, the other training setting is same as (d)'s setting.

The compare methods are the same as (e) and the experimental results have been shown in Table. 5, we could see that our **IAT** also gains the best results on both detection accuracy and test time. For the extensive analyses, we also tried to initialise the IAT module with a weight of exposure dataset [1], but found it did not contribute to the model training (see IAT(exp) in Table. 5).

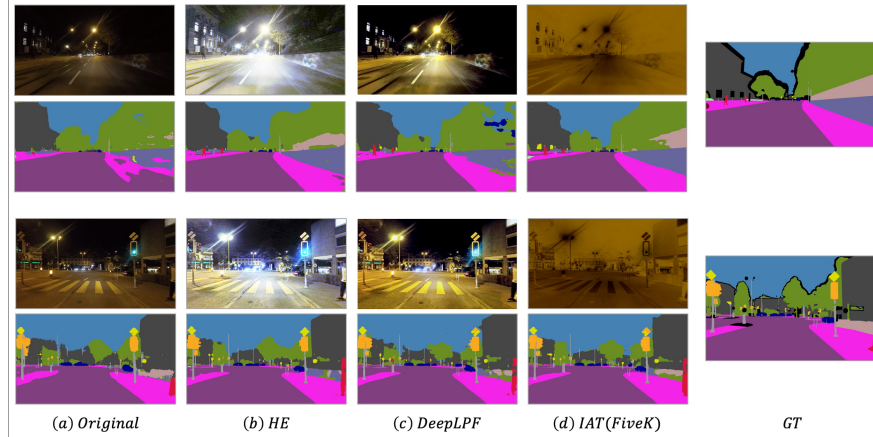


Fig. 7. Segmentation results of DeepLabV3+ [12] on ACDC [56]. (a) is the original images, (b) and (c) are images enhancement by HE method and DeepLPF, (d) are the output of IAT model ($I_t(x)$ in Eq. 7), initialed by FiveK [6].

Table 6. Experiments on LOL [65] dataset (SSIM, PSNR) and EXDark [46] dataset (mAP), shows each part’s contribution of IAT.

Local Branch	Layer Norm	[60]’s Norm	Our Norm	Global Norm	Global (matrix)	Global (gamma)	PSNR↑	SSIM↑	mAP↑
√	√						18.80	0.762	75.8
√		√					19.61 (+0.81)	0.776 (+0.014)	75.8 (+0.0)
√			√				20.01 (+1.21)	0.786 (+0.024)	76.3 (+0.5)
√		√	√				21.95 (+3.15)	0.811 (+0.049)	76.5 (+0.7)
√		√		√			22.76 (+3.96)	0.805 (+0.043)	76.7 (+0.9)
√		√	√	√			23.50 (+4.70)	0.824 (+0.062)	77.1 (+1.3)

4.4 Ablation Analysis

Contribution of each part. To evaluate each part’s contribution in our IAT model, we make an ablation study on the low-light enhancement task of LOL [65] dataset, and the low-light object detection task of EXDark [46] dataset. We report the PSNR and SSIM results of the enhancement task and the mAP result of the detection task. We compare our normalization type with LayerNorm [2] and ResMLP’s normalization [60], and then evaluate different parts’ contributions of the global branch (predict matrix and predict gamma value). The ablation results are shown in Table. 6.

Blocks & Channels Ablation. To evaluate the scalability of our IAT model, we try the different block numbers and channel numbers in the local branch. We try different PEM numbers to generate M and A . The PSNR results on LOL [65] dataset has been shown in Table.7. It shows that keeping the same PEM number to generate M and A would be helpful to IAT’s performance.

Keeping the same block number to generate M and A , we then evaluate with similar parameters to answer whether the local branch should be “short and thick” or “long and thin”. The local branch’s block number and channel

Table 7. Blocks Number.

$M \backslash A$	2	3	4
2	22.10	22.85	22.34
3	22.24	23.50	22.67
4	22.42	23.00	23.48

Table 8. Channel Number.

#Channel:#Block	PSNR \uparrow	SSIM \uparrow	#Param. \downarrow (K)
Short and Thick (12:4)	22.60	0.807	86.22
Long and Thin (24:2)	22.70	0.815	101.03
Ours (16:3)	23.50	0.824	91.15

number are respectively set to 2/24 and 4/12 for comparison. The results of PSNR, SSIM and model parameters are reported in Table. 8.

5 Conclusion

Explicitly considering the ISP pipeline in the camera, we have proposed a novel framework IAT for challenging light conditions. Despite its superior performance on several real-world datasets for both low-level and high-level tasks, IAT is extremely lightweight with a fast speed. The lightweight and mobile-friendly IAT has the potential to become a standing plug-in tool for the computer vision community.

References

1. Afifi, M., Derpanis, K.G., Ommer, B., Brown, M.S.: Learning multi-scale photo exposure correction. In: Proceedings of the IEEE/CVF Conference on Computer Vision and Pattern Recognition (2021)
2. Ba, J., Kiros, J.R., Hinton, G.E.: Layer normalization. ArXiv [abs/1607.06450](https://arxiv.org/abs/1607.06450) (2016)
3. Bianco, S., Cusano, C., Schettini, R.: Single and multiple illuminant estimation using convolutional neural networks. IEEE Transactions on Image Processing (2017)
4. Brainard, D.H., Wandell, B.A.: Analysis of the retinex theory of color vision. JOSA A (1986)
5. Brooks, T., Mildenhall, B., Xue, T., Chen, J., Sharlet, D., Barron, J.T.: Unprocessing images for learned raw denoising. In: Proceedings of the IEEE Conference on Computer Vision and Pattern Recognition (2019)
6. Bychkovsky, V., Paris, S., Chan, E., Durand, F.: Learning photographic global tonal adjustment with a database of input / output image pairs. In: Proceedings of the IEEE Conference on Computer Vision and Pattern Recognition (2011)
7. Carion, N., Massa, F., Synnaeve, G., Usunier, N., Kirillov, A., Zagoruyko, S.: End-to-end object detection with transformers. In: European conference on computer vision (2020)
8. Celik, T., Tjahjadi, T.: Contextual and variational contrast enhancement. IEEE Transactions on Image Processing (2011)
9. Chen, C., Chen, Q., Xu, J., Koltun, V.: Learning to see in the dark. In: IEEE/CVF Conference on Computer Vision and Pattern Recognition (2018)
10. Chen, H., Wang, Y., Guo, T., Xu, C., Deng, Y., Liu, Z., Ma, S., Xu, C., Xu, C., Gao, W.: Pre-trained image processing transformer. In: Proceedings of the IEEE/CVF Conference on Computer Vision and Pattern Recognition (2021)

11. Chen, K., Wang, J., Pang, J., Cao, Y., Xiong, Y., Li, X., Sun, S., Feng, W., Liu, Z., Xu, J., Zhang, Z., Cheng, D., Zhu, C., Cheng, T., Zhao, Q., Li, B., Lu, X., Zhu, R., Wu, Y., Dai, J., Wang, J., Shi, J., Ouyang, W., Loy, C.C., Lin, D.: MMDetection: Open mmlab detection toolbox and benchmark. arXiv preprint arXiv:1906.07155 (2019)
12. Chen, L.C., Zhu, Y., Papandreou, G., Schroff, F., Adam, H.: Encoder-decoder with atrous separable convolution for semantic image segmentation. In: Proceedings of the European conference on computer vision (2018)
13. Chen, S., Feng, H., Gao, K., Xu, Z., Chen, Y.: Extreme-quality computational imaging via degradation framework. In: Proceedings of the IEEE/CVF International Conference on Computer Vision (2021)
14. Chen, Y.S., Wang, Y.C., Kao, M.H., Chuang, Y.Y.: Deep photo enhancer: Unpaired learning for image enhancement from photographs with gans. In: IEEE/CVF Conference on Computer Vision and Pattern Recognition (2018)
15. Contributors, M.: MMSegmentation: Openmmlab semantic segmentation toolbox and benchmark. <https://github.com/open-mmlab/mmsegmentation> (2020)
16. Cui, Z., Qi, G.J., Gu, L., You, S., Zhang, Z., Harada, T.: Multitask aet with orthogonal tangent regularity for dark object detection. In: Proceedings of the IEEE/CVF International Conference on Computer Vision (2021)
17. Deng, J., Dong, W., Socher, R., Li, L.J., Li, K., Fei-Fei, L.: Imagenet: A large-scale hierarchical image database. In: IEEE conference on computer vision and pattern recognition (2009)
18. Dosovitskiy, A., Beyer, L., Kolesnikov, A., Weissenborn, D., Zhai, X., Unterthiner, T., Dehghani, M., Minderer, M., Heigold, G., Gelly, S., Uszkoreit, J., Houlsby, N.: An image is worth 16x16 words: Transformers for image recognition at scale. In: International Conference on Learning Representations (2021)
19. Ebner, M.: Color constancy based on local space average color. *Machine Vision and Applications* **20**, 283–301 (2008)
20. Fu, Y., Hong, Y., Chen, L., You, S.: Le-gan: Unsupervised low-light image enhancement network using attention module and identity invariant loss. *Knowledge-Based Systems* (2022)
21. Gijsenij, A., Lu, R., Gevers, T.: Color constancy for multiple light sources. *IEEE Transactions on Image Processing* (2012)
22. Gonzalez, R.C., Woods, R.E.: *Digital Image Processing* (3rd Edition). Prentice-Hall, Inc., USA (2006)
23. Gu, L., Huynh, C.P., Robles-Kelly, A.: Segmentation and estimation of spatially varying illumination. *IEEE Transactions on Image Processing* (2014)
24. Guo, C., Li, C., Guo, J., Loy, C.C., Hou, J., Kwong, S., Cong, R.: Zero-reference deep curve estimation for low-light image enhancement. In: IEEE/CVF Conference on Computer Vision and Pattern Recognition (2020)
25. Guo, X., Li, Y., Ling, H.: Lime: Low-light image enhancement via illumination map estimation. *IEEE Transactions on Image Processing* (2017)
26. Han, Q., Fan, Z., Dai, Q., Sun, L., Cheng, M.M., Liu, J., Wang, J.: Demystifying local vision transformer: Sparse connectivity, weight sharing, and dynamic weight. arXiv preprint arXiv:2106.04263 (2021)
27. He, K., Zhang, X., Ren, S., Sun, J.: Deep residual learning for image recognition. In: 2016 IEEE Conference on Computer Vision and Pattern Recognition (2016)
28. Heide, F., et.al, S.: Flexisp: A flexible camera image processing framework. *ACM Trans. Graph.* (2014)

29. Hodan, T., Michel, F., Brachmann, E., Kehl, W., GlentBuch, A., Kraft, D., Drost, B., Vidal, J., Ihrke, S., Zabulis, X., et al.: Bop: Benchmark for 6d object pose estimation. In: Proceedings of the European Conference on Computer Vision (2018)
30. Hu, Y., He, H., Xu, C., Wang, B., Lin, S.: Exposure: A white-box photo post-processing framework. ACM Trans. Graph. (2018)
31. Ignatov, A., Kobyshev, N., Timofte, R., Van Gool, L.: Dslr-quality photos on mobile devices with deep convolutional networks. In: Proceedings of the IEEE international conference on computer vision (2017)
32. Jiang, H., Tian, Q., Farrell, J., Wandell, B.A.: Learning the image processing pipeline. IEEE Transactions on Image Processing (2017)
33. Johnson, J., Alahi, A., Fei-Fei, L.: Perceptual losses for real-time style transfer and super-resolution. In: European Conference on Computer Vision (2016)
34. Karaimer, H.C., Brown, M.S.: A software platform for manipulating the camera imaging pipeline. In: European Conference on Computer Vision (2016)
35. Kim, H., Choi, S.M., Kim, C.S., Koh, Y.J.: Representative color transform for image enhancement. In: Proceedings of the IEEE/CVF International Conference on Computer Vision (2021)
36. Kumar, M., Weissenborn, D., Kalchbrenner, N.: Colorization transformer. In: International Conference on Learning Representations (2021)
37. Land, E.H.: An alternative technique for the computation of the designator in the retinex theory of color vision. Proceedings of the National Academy of Sciences of the United States of America (1986)
38. Lee, C., Lee, C., Kim, C.S.: Contrast enhancement based on layered difference representation of 2d histograms. IEEE Transactions on Image Processing (2013)
39. Li, K., Wang, Y., Peng, G., Song, G., Liu, Y., Li, H., Qiao, Y.: Uniformer: Unified transformer for efficient spatial-temporal representation learning. In: International Conference on Learning Representations (2022)
40. Li, K., Wang, Y., Zhang, J., Gao, P., Song, G., Liu, Y., Li, H., Qiao, Y.: Uniformer: Unifying convolution and self-attention for visual recognition. arXiv preprint arXiv:2201.09450 (2022)
41. Liang, J., Cao, J., Sun, G., Zhang, K., Van Gool, L., Timofte, R.: Swinir: Image restoration using swin transformer. In: IEEE International Conference on Computer Vision Workshops (2021)
42. Lin, T.Y., Maire, M., Belongie, S., Hays, J., Perona, P., Ramanan, D., Dollár, P., Zitnick, C.L.: Microsoft coco: Common objects in context. In: European conference on computer vision (2014)
43. Liu, J., Xu, D., Yang, W., Fan, M., Huang, H.: Benchmarking low-light image enhancement and beyond. International Journal of Computer Vision (2021)
44. Liu, W., Ren, G., Yu, R., Guo, S., Zhu, J., Zhang, L.: Image-adaptive yolo for object detection in adverse weather conditions. In: Proceedings of the AAAI Conference on Artificial Intelligence (2022)
45. Liu, Z., Lin, Y., Cao, Y., Hu, H., Wei, Y., Zhang, Z., Lin, S., Guo, B.: Swin transformer: Hierarchical vision transformer using shifted windows. In: Proceedings of the IEEE/CVF International Conference on Computer Vision (2021)
46. Loh, Y.P., Chan, C.S.: Getting to know low-light images with the exclusively dark dataset. Computer Vision and Image Understanding (2019)
47. Lore, K.G., Akintayo, A., Sarkar, S.: Llnet: A deep autoencoder approach to natural low-light image enhancement. Pattern Recognition (2017)
48. Lv, F., Lu, F., Wu, J., Lim, C.: Mbllen: Low-light image/video enhancement using cnns. In: British Machine Vision Conference (2018)

49. Minciullo, L., Manhardt, F., Yoshikawa, K., Meier, S., Tombari, F., Kobori, N.: Db-gan: Boosting object recognition under strong lighting conditions. In: Proceedings of the IEEE/CVF Winter Conference on Applications of Computer Vision (2021)
50. Mittal, A., Soundararajan, R., Bovik, A.C.: Making a “completely blind” image quality analyzer. IEEE Signal processing letters (2012)
51. Moran, S., Marza, P., McDonagh, S., Parisot, S., Slabaugh, G.: Deeplpf: Deep local parametric filters for image enhancement. In: Proceedings of the IEEE/CVF Conference on Computer Vision and Pattern Recognition (2020)
52. Morawski, I., Chen, Y.A., Lin, Y.S., Hsu, W.H.: Nod: Taking a closer look at detection under extreme low-light conditions with night object detection dataset. arXiv preprint arXiv:2110.10364 (2021)
53. Park, J., Lee, J.Y., Yoo, D., Kweon, I.S.: Distort-and-recover: Color enhancement using deep reinforcement learning. In: Proceedings of the IEEE conference on computer vision and pattern recognition (2018)
54. Redmon, J., Farhadi, A.: Yolov3: An incremental improvement. arXiv preprint arXiv:1804.02767 (2018)
55. Ronneberger, O., Fischer, P., Brox, T.: U-net: Convolutional networks for biomedical image segmentation (2015)
56. Sakaridis, C., Dai, D., Van Gool, L.: ACDC: The adverse conditions dataset with correspondences for semantic driving scene understanding. In: Proceedings of the IEEE/CVF International Conference on Computer Vision (2021)
57. Sasagawa, Y., Nagahara, H.: Yolo in the dark: Domain adaptation method for merging multiple models. In: Proceedings of European Conference on Computer Vision (2020)
58. Tolstikhin, I., Houlsby, N., Kolesnikov, A., Beyer, L., Zhai, X., Unterthiner, T., Yung, J., Steiner, A., Keysers, D., Uszkoreit, J., Lucic, M., Dosovitskiy, A.: Mlp-mixer: An all-mlp architecture for vision (2021)
59. Tomasi, C., Manduchi, R.: Bilateral filtering for gray and color images. In: Sixth international conference on computer vision (IEEE Cat. No. 98CH36271) (1998)
60. Touvron, H., Bojanowski, P., Caron, M., Cord, M., El-Nouby, A., Grave, E., Izacard, G., Joulin, A., Synnaeve, G., Verbeek, J., et al.: Resmlp: Feedforward networks for image classification with data-efficient training. arXiv preprint arXiv:2105.03404 (2021)
61. Touvron, H., Cord, M., Sablayrolles, A., Synnaeve, G., Jégou, H.: Going deeper with image transformers. In: Proceedings of the IEEE/CVF International Conference on Computer Vision (2021)
62. Tu, Z., Talebi, H., Zhang, H., Yang, F., Milanfar, P., Bovik, A., Li, Y.: Maxim: Multi-axis mlp for image processing. arXiv preprint arXiv:2201.02973 (2022)
63. Valanarasu, J.M.J., Yasarla, R., Patel, V.M.: Transweather: Transformer-based restoration of images degraded by adverse weather conditions. arXiv preprint arXiv:2111.14813 (2021)
64. Wang, R., Zhang, Q., Fu, C.W., Shen, X., Zheng, W.S., Jia, J.: Underexposed photo enhancement using deep illumination estimation. In: The IEEE Conference on Computer Vision and Pattern Recognition (2019)
65. Wei, C., Wang, W., Yang, W., Liu, J.: Deep retinex decomposition for low-light enhancement. In: British Machine Vision Conference (2018)
66. Yang, W., Yuan, Y., et.al: Advancing image understanding in poor visibility environments: A collective benchmark study. IEEE Transactions on Image Processing (2020)

67. Yang, W., Wang, S., Fang, Y., Wang, Y., Liu, J.: From fidelity to perceptual quality: A semi-supervised approach for low-light image enhancement. In: IEEE/CVF Conference on Computer Vision and Pattern Recognition (2020)
68. Yu, R., Liu, W., Zhang, Y., Qu, Z., Zhao, D., Zhang, B.: Deepexposure: Learning to expose photos with asynchronously reinforced adversarial learning. In: Advances in Neural Information Processing Systems (2018)
69. Yuan, L., Sun, J.: Automatic exposure correction of consumer photographs. In: European Conference on Computer Vision (2012)
70. Zamir, S.W., Arora, A., Khan, S., Hayat, M., Khan, F.S., Yang, M.H.: Restormer: Efficient transformer for high-resolution image restoration. arXiv preprint arXiv:2111.09881 (2021)
71. Zhang, L., Qi, G.J., Wang, L., Luo, J.: Aet vs. aed: Unsupervised representation learning by auto-encoding transformations rather than data. In: Proceedings of the IEEE Conference on Computer Vision and Pattern Recognition (2019)
72. Zhang, Y., Guo, X., Ma, J., Liu, W., Zhang, J.: Beyond brightening low-light images. International Journal of Computer Vision (2021)
73. Zhang, Y., Zhang, J., Guo, X.: Kindling the darkness: A practical low-light image enhancer. In: Proceedings of the 27th ACM international conference on multimedia (2019)
74. Zhang, Z., Jiang, Y., Jiang, J., Wang, X., Luo, P., Gu, J.: Star: A structure-aware lightweight transformer for real-time image enhancement. In: Proceedings of the IEEE/CVF International Conference on Computer Vision (2021)